mechanisms of tissue accumulation and washout of these compounds are not yet fully understood, evidence is emerging that their interaction with subcellular organelles and complex macromolecules might provide a new basis for advancing knowledge in important aspects of tumor biology that bear some relevance to the therapy of cancer patients.

ACKNOWLEDGMENT

The author is indebted to Dr. David Piwnica-Worms (The Mallinckrodt Institute of Radiology, Washington University, St. Louis, MO) for stimulating discussion and offering constructive criticism of this article.

REFERENCES

1. Piwnica-Worms D, Kronauge JF, Holman BL, Davison A, Jones AG. Comparative myocardial uptake characteristics of hexakis (alkylisonitrile) technetium(I) complexes: effect of lipophilicity. *Invest Radiol* 1989;24:25–29.
2. Rossetti C, Vanoli G, Paganelli G, et al. Human biodistribution, dosimetry and clinical use of technetium(III)-99m-Q12. *J Nucl Med* 1994;35:1571–1580.
3. Biniakiewicz DS, Washburn LC, McGoron AJ, Gerson MC. Synthesis and biodistribution of new ^{99m}Tc Q-series complexes with ester functionality [Abstract]. *J Nucl Med* 1995;36(suppl.):17P.
4. Crankshaw CL, Marmion M, Burleigh BD, Deutsch E, Piwnica-Worms D. Nonreducible mixed ligand Tc(III) cations (Q complexes) are recognized as transport substrates by the human multidrug resistance (MDR) P-glycoprotein [Abstract]. *J Nucl Med* 1995;36(suppl.):130P.
5. Wackers FJT. The maze of myocardial perfusion imaging protocols in 1994. *J Nucl Cardiol* 1994;1:180–188.
6. Sharma V, Herman LW, Barbarics E, Rao VV, Kronauge JF, Piwnica-Worms D. Synthesis and initial characterization of novel aryl-isonitrile ^{99m}Tc complexes targeted to the multidrug resistance (MDR) P-glycoprotein [Abstract]. *J Nucl Med* 1995; 36(suppl.):27P–28P.
7. Mansi L, Rambaldi PF, La Provitera A, Di Gregorio F, Procaccini E. Tc-99m Tetrofosmin uptake in breast tumors [Abstract]. *J Nucl Med* 1995;36(suppl.):83P.
8. Ballinger JR, Bannerman J, Boxen I, et al. Accumulation of Tc-99m tetrofosmin in breast tumour cells in vitro: role of multidrug-resistance P-glycoprotein [Abstract]. *J Nucl Med* 1995;36(suppl.):202P.
9. Kronauge JF, Chiu ML, Cone JS, et al. Comparison of neutral and cationic myocardial perfusion agents: characteristics of accumulation in cultured cells. *Nucl Med Biol* 1992;19:141–148.
10. Pasqualini R, Duatti A, Bellande E, et al. Bis(dithiocarbamato) nitrido technetium-99m radiopharmaceuticals: a class of neutral myocardial imaging agents. *J Nucl Med* 1994;35:334–341.
11. Piwnica-Worms D, Kronauge JF, Delmon L, Holman BL, Marsh JD, Jones AG. Effect of metabolic inhibition on technetium-99m-MIBI kinetics in cultured chick myocardial cells. *J Nucl Med* 1990;31:464–472.
12. Carvalho PA, Chiu ML, Kronauge JF, et al. Subcellular distribution and analysis of technetium-99m-MIBI in isolated perfused rat hearts. *J Nucl Med* 1992;33:1516–1521.
13. Piwnica-Worms D, Kronauge JF, Chiu ML. Uptake and retention of hexakis (2-methoxyisobutyl isonitrile) technetium(I) in cultured chick myocardial cells. Mitochondrial and plasma membrane potential dependence. *Circulation* 1990;82:1826–1838.
14. Chernoff DM, Strichartz GR, Piwnica-Worms D. Membrane potential determination in large unilamellar vesicles with haxakis(2-methoxyisobutyl-isonitrile)technetium(I). *Biochim Biophys Acta* 1993;1147:262–266.
15. Delmon-Moingeon LI, Piwnica-Worms D, Van den Abbeele AD, Holman BL, Davison A, Jones AG. Uptake of the cation hexakis(2-methoxyisobutylisonitrile)-technetium-99m by human carcinoma cell lines in vitro. *Cancer Res* 1990;50:2198–2202.
16. Chiu ML, Kronauge JF, Piwnica-Worms D. Effect of mitochondrial and plasma membrane potentials on accumulation of hexakis (2-methoxyisobutylisonitrile) technetium(I) in cultured mouse fibroblasts. *J Nucl Med* 1990;31:1646–1653.
17. Piwnica-Worms D, Kronauge JF, Chiu ML. Enhancement by tetraphenylborate of technetium-99m-MIBI uptake kinetics and accumulation in cultured chick myocardial cells. *J Nucl Med* 1991;32:1992–1999.
18. Piwnica-Worms D, Chiu ML, Kronauge JF. Divergent kinetics of ^{201}Tl and ^{99m}Tc-sestamibi in cultured chick ventricular myocytes during ATP depletion. *Circulation* 1992;85:1531–1541.
19. Piwnica-Worms D, Kronauge JF, LeFurgey A, et al. Mitochondrial localization and characterization of ^{99}Tc-Sestamibi in heart cells by electron probe x-ray microanalysis and ^{99}Tc NMR spectroscopy. *Magn Res Imag* 1994;12:641–652.
20. Cesani F, Ernst R, Walser E, Villanueva-Meyer J. Technetium-99m sestamibi imaging of a pancreatic VIPoma and parathyroid adenoma in a patient with multiple type I endocrine neoplasia. *Clin Nucl Med* 1994;19:532–534.
21. Al-Sebaie S, Rush C. Liver metastases detected by ^{99m}Tc sestamibi during routine cardiac imaging. *Clin Nucl Med* 1995;20:84–85.
22. Abdel-Dayem HM, Scott AM, Macapinlac HA, El-Gazzar AH, Larson SM. Role of thallium-201-chloride and ^{99m}Tc-sestamibi in tumor imaging. In: Freeman LM, ed. *Nuclear Medicine Annual 1994.* New York: Raven Press; 1994:181–234.
23. Moscow JA, Cowan KH. Multidrug resistance. *J Natl Cancer Inst* 1988;80:14–20.
24. Goldstein LJ, Galski H, Fojo A, et al. Expression of a multidrug resistance gene in human cancers. *J Natl Cancer Inst* 1989;81:116–124.
25. Deuchars KL, Ling V. P-Glycoprotein and multidrug resistance in cancer chemotherapy. *Semin Oncol* 1989;16:156–165.
26. Ford JM, Hait WN. Pharmacology of drugs that alter multidrug resistance in cancer. *Pharmacol Rev* 1990;42:155–199.
27. Piwnica-Worms D, Chiu ML, Budding M, Kronauge JF, Kramer RA, Croop JM. Functional imaging of multidrug-resistant P-glycoprotein with an organotechnetium complex. *Cancer Res* 1993;53:977–984.
28. Rogan AM, Hamilton TC, Young RC, Klecker RW, Ozols RF. Reversal of adriamycin resistance by verapamil in human ovarian cancer. *Science* 1984;224:994–996.
29. Ozols RF, Cunnian RE, Klecker RW, et al. Verapamil and adriamycin in the treatment of drug-resistant ovarian cancer patients. *J Clin Oncol* 1987;5:641–647.
30. Miller TP, Grogan TM, Dalton WS, et al. P-Glycoprotein expression in malignant lymphoma and reversal of clinical drug resistance with chemotherapy plus high-dose verapamil. *J Clin Oncol* 1991;9:17–24.
31. Sonneveld P, Durian BG, Lokhorst HM, Marie J-P, et al. Modulation of multidrug-resistant multiple myeloma by cyclosporin. *Lancet* 1992;340:255–259.
32. Moretti JL, Caglar M, Duran-Cordobes M, Morere J-F. Can nuclear medicine predict response to chemotherapy? *Eur J Nucl Med* 1995;22:97–100.
33. Moretti JL, Caglar M, Boaziz C, Caillat-Vigneron N, Morere J-F. Sequential functional imaging with technetium-99m-hexakis-2-methoxyisobutylisonitrile and indium-111-octreotide: can we predict the response to chemotherapy in small cell lung cancer? *Eur J Nucl Med* 1995;22:177–180.
34. Dimitrakopoulou-Strauss A, Strauss LG, Goldschmidt H, et al. Evaluation of tumour metabolism and multidrug resistance in patients with treated malignant lymphomas. *Eur J Nucl Med* 1995;22:434–442.
35. Ciarmiello A, Del Vecchio S, Potena MI, et al. Technetium-99m-sestamibi efflux and P-glycoprotein expression in human breast carcinoma [Abstract]. *J Nucl Med* 1995; 36(suppl.):129P.

MIRDOSE: Personal Computer Software for Internal Dose Assessment in Nuclear Medicine

Michael G. Stabin

Oak Ridge Institute for Science and Education, Oak Ridge, Tennessee

Key Words: internal dosimetry; computers

J Nucl Med 1996; 37:538–546

The calculation of internal dose estimates is performed by summing the radiation absorbed in various target tissues from a number of source organs in the body that contain significant quantities of radioactive material. In nuclear medicine, the most commonly used method for the calculation of internal dose estimates is that developed by the Medical Internal Radiation Dose (MIRD) committee, as described in various documents, but most recently summarized in the MIRD Primer (*1*). In this article, the expression given for the absorbed dose is:

$$D_k = A_0 \sum_j \tau_j \sum_i \frac{\Delta_i \phi(r_k \leftarrow r_j)_i}{m_k}, \qquad \text{Eq. 1}$$

Received Jul. 28, 1995; revision accepted Jul. 29, 1995.

For correspondence or reprints contact: Michael G. Stabin, Radiation Internal Dose Information Center, Oak Ridge Institute for Science and Education, P.O. Box 117, Oak Ridge, TN 37831.

where D_k is the mean absorbed dose to region k (Gy); A_0 is the administered activity (Bq); τ_j is the residence time in source region j (s); Δ_i is the mean energy emitted per nuclear decay for emission type i (Gy-kg/Bq-s); $\phi_i(r_k \leftarrow r_j)$ is the fraction of energy emitted in source region j which is absorbed in target region k; and m_k is the mass of target region k (kg).

The residence time for a source region is the ratio of the cumulated activity (the total number of disintegrations) to the initial activity in the region. The units are time; typical cumulated activity units are Bq-s, and units for the initial activity are typically Bq.

One may also see the ratio of the absorbed fraction $\phi(r_k \leftarrow r_j)$ over the mass m_k given as the *specific* absorbed fraction $\Phi(r_k \leftarrow r_j)$. The quantity $\Sigma \Delta_i \phi_i(r_k \leftarrow r_j)/m_k$ is often referred to as the S-value (for region j irradiating region k).

A number of the parameters in this expression are rather tedious to look up and evaluate on a routine basis, and thus lend themselves well to treatment with computer programs. The summations also involve repetitive tasks that are best done by computer, leaving the analyst free to devote energy to more creative tasks. Therefore, the MIRDOSE computer software was developed several years ago (*2*) and has been continually supported and updated since then.

Although the software was originally described in the proceedings of a Midyear Meeting of the Health Physics Society (*2*), and has been distributed around the world with some limited documentation, the software has never been fully described in the open literature. Such a description serves two purposes: (a) it provides the current technical basis for the software and (b) it permits the citation of the software in an open literature reference for users who wish to use it to perform dose assessment in publications or other documents.

In addition, this article outlines some of the important differences between versions 2 and 3 of the program to help users understand variations in program output between the two versions and any effect this might have on their work.

STRUCTURE OF THE PROGRAM

Overview

The main function of the program is to provide estimates of the radiation dose per unit administered activity from user-entered source organ residence times for a given radionuclide and one or more phantoms. The program uses libraries of radionuclide decay data and specific absorbed fractions to develop S-values for the source organs chosen by the user and the target organs desired. The estimates of radiation dose per unit administered activity are given in SI and traditional units, with the two organs contributing the first and second highest percentages of the total dose; all source organ contributions to total dose may be viewed if desired. All model input and assumptions are given with the program output. The program will also provide tables of S-values for all source and target organs for a given phantom or phantoms if desired, in lieu of radiation dose estimates.

Program Data Libraries

The two major datasets needed to use Equation 1, given a set of source organ residence times, are the radionuclide decay data and the specific absorbed fractions for the various phantoms of interest. In version 2 of the program, 59 radionuclides were available (Table 1). Decay data were taken from several sources; the main source was a preliminary version of the data which was eventually published as the *MIRD: Radionuclide Data and Decay Schemes* (*3*). Some other data, however, were taken from a document by David Kocher (*4*) and *ICRP Publication 38* (*5*). These data were entered manually and proofread, and some selection was made of the number of important emissions. In version 3, all of the radionuclides in the *MIRD: Radionuclide Data and Decay Schemes* (*3*), except for those including alpha or spontaneous fission decays, were electronically transferred into the program data files (Table 2). Generally, the authors of this publication omitted transitions that did not contribute more than 0.1% to the total energy per transition in that category of emission (*3*).

Two major classes of emissions were considered in version 2: photons ("penetrating" emissions) and electrons and beta particles ("nonpenetrating" emissions). In addition, a third class of emission was derived, which usually constituted a minor contribution to overall dose; this category included any x- or gamma-rays with energy below 10 keV. These photons were treated as "nonpenetrating" emissions in that they were generally absorbed where they were emitted; they were given a different classification so that they would not be treated as electrons in the electron dose models for bone and marrow (described below). In version 3, this classification scheme was continued with the modification that beta particles were distinguished from monoenergetic electrons for use in the calculation of dose to small spheres, as required by the model used to calculate dose to small, unit density spheres (see Special Models And Features, below). The inclusion of alpha emitters was intentionally avoided, as alpha emitters have not been used much in nuclear medicine and because their introduction caused an increase in program complexity. The use of some alpha emitters in antibody therapy has prompted consideration of inclusion of this feature in future versions.

In both versions 2 and 3, the pediatric phantom series of Cristy and Eckerman (*6*) was used for the photon-specific absorbed fraction libraries, giving the user the ability to calculate dose estimates for adults (70 kg), 15-yr-olds (57 kg), 10-yr-olds (32 kg), 5-yr-olds (19 kg), 1-yr-olds (9.2 kg) and newborns (3.4 kg).

The model for the 15-yr-old has been used often as an adult female reference model. These phantoms were designed to take into account the size, shape and position of the various organs at the different ages based on available literature. The masses of these phantoms and of the organ regions in each phantom are shown in Table 3. The bone marrow in the models changes considerably with age. In the newborn, the active marrow is distributed throughout the entire length of the long bones, as well as in the other bones of the skeleton. With age, the long bones contain less and less active marrow and more and more inactive, or yellow, marrow. Thus, it is questionable whether the model for the 15-yr-old should be used for the adult female. In reviewing these data, however, it was felt that the individual variation in marrow location and mass in adult women was as great, or greater, than the difference between the 15-yr-old and the adult phantoms, and that the approximation was reasonable. Thus, it was used in this fashion for a number of years.

In version 3, the pregnant female phantom series of Stabin et al. (*7*) was added to the software. These phantoms were designed to represent the adult female at different stages of pregnancy. In addition, this series included a specific model for the adult female different from the 15-yr-old Cristy/Eckerman phantom. The organ masses are based on those suggested in *ICRP Publication 23* (*8*) for the adult female. The specific absorbed fractions for the 15-yr-old were modified in the case of organ self-irradiation to account for these mass differences, while specific absorbed fractions for organ cross-irradiation were left unchanged. The bone and marrow model for the 15-yr-old was also used to represent the adult female. The

TABLE 1
Radionuclides Available in MIRDOSE 2

^{3}H	^{42}K	^{60}Co	^{90}Y	^{127}Xe	^{192}Ir
^{11}C	^{43}K	^{66}Ga	^{97}Ru	^{129}I	^{195}Au
^{13}N	^{45}Ca	^{67}Ga	^{99m}Tc	^{130}I	^{195}Hg
^{14}C	^{51}Cr	^{68}Ga	^{111}In	^{131}I	^{195m}Pt
^{15}O	^{52}Fe	^{72}Ga	^{113m}In	^{133}Xe	^{197}Hg
^{18}F	^{52m}Mn	^{73}Se	^{123m}Te	^{129}Cs	^{198}Au
^{22}Na	^{52}Mn	^{75}Se	^{123}I	^{137}Cs	^{201}Tl
^{24}Na	^{57}Co	^{81m}Kr	^{124}I	^{157}Dy	^{203}Hg
^{32}P	^{58}Co	^{81}Rb	^{125}I	^{169}Yb	^{203}Pb
^{35}S	^{59}Fe	^{82}Rb	^{126}I	^{178}W	

masses of the adult female and the pregnant female phantoms are shown in Table 4.

Specific absorbed fractions for electrons and beta particles (plus and minus) are estimated based on the rules laid out in *MIRD Pamphlet No. 11* (*9*) for "nonpenetrating" emissions and the masses of the target regions in the various phantoms (Tables 3 and 4). Basically, the absorbed fraction is set to 1.0 when the source and target are the same and to 0.0 when they are different, with a few exceptions. Those exceptions include:

1. When the source organ is the contents of a hollow organ and the target is organ wall.
2. When the source or the target organ is the total body.
3. When the source organ is in the bone or marrow and the target organ is one in which crossfire can occur in this region.

The equations for the first two exceptions are given in *MIRD Pamphlet No. 11* (*9*). For bone and marrow, versions 2 and 3 are completely different. In version 2, the model for bone and marrow in *ICRP Publication 30* (*10*) was adopted, as it was felt that this was the model that would be widely used by many segments of the radiation protection community. With experience with this model and examination of its assumptions, however, it became apparent that it was considerably conservative and that the more accurate model developed by Eckerman (*11*) would be much more useful in nuclear medicine. A description of the new bone and marrow model is given in the article by Eckerman and Stabin (*12*), but a brief description and summary of some of the pertinent results will be presented (see section on Special Models and Features).

Calculational Framework

In version 2, only one phantom could be chosen at a time. In version 3, all six phantoms in the pediatric phantom series or all four phantoms in the pregnant female phantom series used with a given choice of radionuclide and set of residence times. For a given phantom, after the program receives all needed input, it proceeds to estimate the S-values it needs to calculate all of the dose estimates needed, as in Equation 1.

Starting with the first source organ, S-values are calculated for each target organ, considering each emission in the decay scheme separately. In version 2, the user was asked to specify the target organs to be studied; in version 3 the program automatically calculates dose to all 26 available target organs. If the emission is a "nonpenetrating" emission, its energy is absorbed locally as described in the rules for these emissions in *MIRD Pamphlet 11* (see above).

After all radionuclide emissions are considered, the total S-value for a source/target organ combination is stored in the S-value matrix in the proper position, and the next target organ is considered. Then, the next source organ is considered until all the needed S-values are calculated.

TABLE 2
Radionuclides Available in MIRDOSE 3

^{3}H	^{67}Cu	^{95}Nb	^{131}Cs	^{195}Au
^{7}Be	^{62}Zn	^{95m}Nb	^{132}Cs	^{195m}Au
^{11}C	^{65}Zn	^{99}Mo	^{134}Cs	^{198}Au
^{14}C	^{69}Zn	^{94m}Tc	^{134m}Cs	^{199}Au
^{13}N	^{69m}Zn	^{95}Tc	^{137}Cs	^{195}Hg
^{14}O	^{66}Ga	^{95m}Tc	^{128}Ba	^{195m}Hg
^{15}O	^{67}Ga	^{97m}Tc	^{131m}Ba	^{197}Hg
^{19}O	^{68}Ga	^{99}Tc	^{133}Ba	^{197m}Hg
^{18}F	^{72}Ga	^{99m}Tc	^{135m}Ba	^{203}Hg
^{19}Ne	^{68}Ge	^{97}Ru	^{137m}Ba	^{206}Hg
^{22}Na	^{72}As	^{103}Ru	^{134}La	^{200}Tl
^{24}Na	^{73}As	^{103m}Rh	^{140}La	^{201}Tl
^{28}Mg	^{74}As	^{103}Pd	^{134}Ce	^{202}Tl
^{28}Al	^{72}Se	^{109}Pd	^{139}Ce	^{206}Tl
^{30}P	^{73}Se	^{109m}Ag	^{141}Ce	^{208}Tl
^{32}P	^{73m}Se	^{109}Cd	^{145}Pm	^{210}Tl
^{33}P	^{75}Se	^{109}In	^{147}Pm	^{201}Pb
^{35}S	^{77m}Se	^{111}In	^{145}Sm	^{203}Pb
^{38}Cl	^{75}Br	^{111m}In	^{153}Sm	^{204m}Pb
^{37}Ar	^{76}Br	^{113m}In	^{154}Eu	^{212}Pb
^{38}K	^{77}Br	^{114}In	^{153}Gd	^{214}Pb
^{40}K	^{80}Br	^{114m}In	^{157}Dy	^{204}Bi
^{42}K	^{80m}Br	^{115m}In	^{159}Dy	^{208}Bi
^{43}K	^{82}Br	^{113}Sn	^{165}Dy	
^{45}Ca	^{77}Kr	^{117m}Sn	^{165}Er	
^{47}Ca	^{79}Kr	^{118}Sb	^{167m}Er	
^{49}Ca	^{81}Kr	^{118m}Sb	^{171}Er	
^{46}Sc	^{81m}Kr	^{123}Te	^{167}Tm	
^{47}Sc	^{83m}Kr	^{123m}Te	^{170}Tm	
^{49}Sc	^{85}Kr	^{122}I	^{171}Tm	
^{48}V	^{85m}Kr	^{123}I	^{169}Yb	
^{48}Cr	^{77}Rb	^{124}I	^{177}Ta	
^{51}Cr	^{79}Rb	^{125}I	^{178}Ta	
^{51}Mn	^{81}Rb	^{126}I	^{179}Ta	
^{52}Mn	^{82}Rb	^{129}I	^{182}Ta	
^{52m}Mn	^{82m}Rb	^{130}I	^{177}W	
^{54}Mn	^{83}Rb	^{131}I	^{178}W	
^{52}Fe	^{84}Rb	^{132}I	^{181}W	
^{55}Fe	^{86}Rb	^{132m}I	^{188}W	
^{59}Fe	^{82}Sr	^{133}I	^{186}Re	
^{55}Co	^{83}Sr	^{122}Xe	^{188}Re	
^{56}Co	^{85}Sr	^{123}Xe	^{190m}Os	
^{57}Co	^{85m}Sr	^{127}Xe	^{191}Os	
^{58}Co	^{87m}Sr	^{129m}Xe	^{191m}Os	
^{60}Co	^{89}Sr	^{131m}Xe	^{190}Ir	
^{57}Ni	^{90}Sr	^{133}Xe	$^{190m1}Ir$	
^{63}Ni	^{87}Y	^{133m}Xe	$^{190m2}Ir$	
^{57}Cu	^{88}Y	^{128}Cs	^{191m}Ir	
^{62}Cu	^{90}Y	^{129}Cs	^{192}Ir	
^{64}Cu	^{95}Zr	^{130}Cs	^{195m}Pt	

After calculation of the S-values, the program checks to see if the S-values for total body as a source need to be corrected to be S-values for the "remainder of the body," i.e., the total body minus any source organs. This option is invoked if "total body" is chosen as a source along with any other organs. If "total body" is the only source chosen, or if it is not chosen at all, this option is not used.

In version 3, the name of the source organ on the input screen changes from "total body" to "remainder of the body" if any other source organs are chosen to attempt to alert the user that the residence time for the "remainder of the body" is expected for this entry. In version 2, "remainder of the body" is shown when the residence time is requested. The S-values for total body as a source are corrected according to the following formula (*13*):

TABLE 3
Masses of Source Regions in the Cristy and Eckerman Phantom Series

Organ	Mass (g) of organ in each phantom					
	Newborn* 3.4 kg	1 yr 9.8 kg	5 yr 19 kg	10 yr 32 kg	15 yr† 55–58 kg	Adult male 70 kg
Adrenals	5.83	3.52	5.27	7.22	10.5	16.3
Brain	352	884	1260	1360	1410	1420
Breasts (including skin)	0.205	1.10	2.17	3.65	407	403
Breasts (excluding skin)	0.107	0.732	1.51	2.60	361	351
Gallbladder contents	2.12	4.81	19.7	38.5	49.0	55.7
Gallbladder wall	0.408	0.910	3.73	7.28	9.27	10.5
GI tract						
LLI contents	6.98	18.3	36.6	61.7	109	143
LLI wall	7.98	20.6	41.4	70.0	127	167
SI contents and wall	52.9	138	275	465	838	1100
stomach contents	10.6	36.2	75.1	133	195	260
stomach wall	6.41	21.8	49.1	85.1	118	158
ULI contents	11.2	28.7	57.9	97.5	176	232
ULI wall	10.5	27.8	55.2	93.4	168	220
Heart contents	36.5	72.7	134	219	347	454
Heart wall	25.4	50.6	92.8	151	241	316
Kidneys	22.9	62.9	116	173	248	299
Liver	121	292	584	887	1400	1910
Lungs	50.6	143	290	453	651	1000
Ovaries	0.328	0.714	1.73	3.13	10.5	8.71
Pancreas	2.80	10.3	23.6	30.0	64.9	94.3
Remaining tissue	2360	6400	13300	23100	40000	51800
Skeleton						
Active marrow	47	150	320	610	1050	1120
Cortical bone	0	299	875	1580	3220	4000
Trabecular bone	140	200	219	396	806	1000
Skin	118	271	538	888	2150	3010
Spleen	9.11	25.5	48.3	77.4	123	183
Testes	0.843	1.21	1.63	1.89	15.5	39.1
Thymus	11.3	22.9	29.6	31.4	28.4	20.9
Thyroid	1.29	1.78	3.45	7.93	12.4	20.7
Urinary bladder contents	12.4	32.9	64.7	103	160	211
Urinary bladder wall	2.88	7.70	14.5	23.2	35.9	47.6
Uterus	3.85	1.45	2.70	4.16	79.0	79.0
Whole body	3600	9720	19800	33200	56800	73700

*Phantom and total phantom weight.
†Also used as adult female phantom.

$$S(r_k \leftarrow RB) = S(r_k \leftarrow TB)\left(\frac{m_{TB}}{m_{RB}}\right) - \sum_h S(r_k \leftarrow r_h)\left(\frac{m_h}{m_{RB}}\right),$$

where $S(r_k \leftarrow RB)$ is the S-value for remainder of the body irradiating target region r_k; $S(r_k \leftarrow TB)$ is the S-value for the total body irradiating target region r_k; $S(r_k \leftarrow r_h)$ is the S-value for source region h irradiating target region r_k; m_{TB} is the mass of the total body; m_{RB} is the mass of the remainder of the body, i.e., the total body minus all other source organs used in this problem; and m_h is the mass of source region h.

After all corrected S-values are available, the program simply loops over all of the source organs for each target organ, calculating the individual contributions to dose and the total dose. Each contribution to an organ's total dose is saved in a matrix so that the individual contributors may be identified in a subsequent search routine. After printing a header in which the program version is displayed, along with a notation of the user's chosen radionuclide, program output label and the date, the program proceeds one target organ at a time and prints or displays the results for each target organ as it is calculated.

In version 2, the only output option was to print to the computer's LPT1: printer port; if no printer was available, the program would end with an error status. This limitation was removed in version 3 as the user may view the results on the screen, print them or send them to a disk file for later use. In version 3, the results are automatically shown on the screen, with options available to send the results to a file or the default printer.

With any program output in either version 2 or 3, all of the organ residence times are listed below the program output, as well as the assumptions used in either the Dynamic Bladder Model or ICRP 30 GI Tract Model (see section Special Models and Features), if used. The user also has the option, in either version, to look at all source organ contributions to a target organ's total dose; if this option is chosen, this output will be included on any program output. In version 3, the user also has the option of looking next at dose estimates for other phantoms which were initially chosen for study. If this output is to be sent to a file or printer, its output will follow that for the previous phantom; all of the above information about residence times and model assumptions will be printed again with the output.

Production of S-Value Tables

If, instead of dose estimates, the user simply wants to produce a complete table of S-values for the radionuclide and phan-

TABLE 4
Masses of Source Regions in the Pregnant Female Phantom Series

Organ	Mass (g) of organ in each phantom			
	Adult female (nonpregnant)	Three-month pregnant female	Six-month pregnant female	Nine-month pregnant female
Adrenals	14	14	14	14
Brain	1200	1200	1200	1200
Breasts (excluding skin)	360	360	360	360
Gallbladder contents	50	50	50	50
Gallbladder wall	8	8	8	8
LLI contents	135	135	135	135
LLI wall	160	160	160	160
Small intestine contents	375	375	375	375
Small intestine wall	600	600	600	600
Stomach contents	230	230	230	230
Stomach wall	140	140	140	140
ULI contents	210	210	210	210
ULI wall	200	200	200	200
Heart contents	410	410	410	410
Heart wall	240	240	240	240
Kidneys	275	275	275	275
Liver	1400	1400	1400	1400
Lungs	651	651	651	651
Ovaries	11	11	11	11
Pancreas	85	85	85	85
Remaining tissue*	40000	39300	41700	39500
Skeleton				
Active marrow	1300	1300	1300	1300
Cortical bone	3000	3000	3000	3000
Trabecular bone	750	750	750	750
Skin	1790	1790	1790	1790
Spleen	150	150	150	150
Thymus	20	20	20	20
Thyroid	17	17	17	17
Urinary bladder contents	160	128	107	42.3
Urinary bladder wall	35.9	36.9	34.5	23.9
Uterine wall	80	374	834	1095
Fetus	—	458	1640	2960
Placenta	—	—	310	466
Whole body	58000	58000	61500	63700
Whole body (maternal tissues)	56800	56400	57500	56600

*Remaining tissue is defined as the part of the phantom remaining when all defined organs have been removed. This region of the phantom has been used in the radiation transport code to model muscle for dosimetric purposes. The appropriate mass of muscle to use in such calculations in the adult female, however, is 15,500 g. The entries for this region have been rounded to two significant figures.

tom(s) chosen, that may be done by selecting this pathway. It is helpful to have all of the S-values printed on one or two pages, with columns of values for each source organ. With 24–27 source organs available, this results in the need for printing 12–14 columns per page.

Printing these results is problematic because many different printers are available. For this reason, version 2 was distributed with copies of the source code so that modifications could be made by the user to allow the S-value table to be printed in compressed print on any individual printer. In version 3, the S-values were simply printed in fewer columns, therefore using more pages and the standard printer handling routines were considered adequate. For this reason, the source code was not distributed with version 3 and is not available. Output of S-values to a file is also permitted so that the user may adapt the source output to any format using available editors.

Special Models and Features

Plot Program. Version 2 was released with a program that performed simple least-squares fitting of data to functions involving one, two or three exponential terms. The purpose of this routine was to permit the user to calculate residence times, given a set of bioretention data. The program asked the user to enter activity for times at which measurements were taken and the corresponding values of measured activity. The program then fit the data to the desired number of exponential terms, using standard least squares methodology (*14*). The program returned the values of a and b for the following equation:

$$A(t) = a_1 e^{-b_1 t} + a_2 e^{-b_2 t} + \ldots, \qquad \text{Eq. 3}$$

where A(t) is the activity at time t; a_i is the amount of activity associated with component i; and b_i is the rate coefficient for clearance of component i, (hr^{-1}). $b_i = 0.693/T_i$, where T_i is the half-time for clearance of component i (hr).

If this expression is integrated to infinity, the residence time may be quickly estimated as:

$$\tau = \frac{a_1}{b_1} + \frac{a_2}{b_2} + \ldots, \qquad \text{Eq. 4}$$

TABLE 5
Residence Times (HR) in the Gastrointestinal Tract at Various Ages

GI tract segment	Phantom					
	Newborn	1-yr-old	5-yr-old	10-yr-old	15-yr-old	Adult*
Stomach	0.5	0.5	1.0	1.0	1.0	1.0
Small intestine	0.58	0.78	3.1	4.0	4.0	4.0
Upper large intestine	1.9	2.54	10.2	13.0	13.0	13.0
Lower large intestine	3.5	4.68	18.8	24.0	24.0	24.0

*These values used for the adult and pregnant female cases.

where τ is the residence time (hr).

This expression assumes that the rate coefficient as defined above represents the sum of biological and physical elimination (the effective removal coefficient).

ICRP 30 Gastrointestinal Tract Model

In *ICRP Publication 30* (*10*), a model for material transport through the gastrointestinal (GI) tract was proposed. In this model, material was assumed to enter the stomach and pass to the small intestine (SI), upper large intestine (ULI), lower large intestine (LLI) and be excreted in the feces at standard rates. Absorption from the SI into the blood was also allowed by the model. This model was implemented in both versions 2 and 3 to be used in cases in which activity in the GI tract was assumed to follow these kinetics.

In addition, activity was permitted to also enter the SI and pass through the rest of the system at the standard rates, to represent cases in which activity entered the GI tract from the liver. The GI transit times were based on measurements in adults and were thought to be too long to represent children. No published values of GI transit rates for children of different ages could be located. Discussions with various pediatricians, however, permitted estimation of total GI transit times in children of different ages. These total GI transit times were then scaled for each of the segments of the GI tract below the stomach in proportion to the values used for adults. The GI transit times used for the different ages are shown in Table 5.

Dynamic Bladder Model

A mathematical model which predicted the total number of disintegrations occurring in the urinary bladder, assuming input into the bladder based on a sum of exponential terms and a regular voiding pattern, was given by Cloutier et al. (*15*). This model was implemented in both versions of the software. The user was asked for the number of components to the input function (number of exponential terms) and for the fraction of injected activity and the biological half-time for clearance for each of the terms. The program then calculated the residence time in the bladder according to the formula given in this model.

Region-Specific Bone and Marrow Model

In version 3, the new bone and marrow model of Eckerman (*11*) for electron dose to bone surfaces and marrow from sources in the trabecular or cortical bone was implemented. This replaced the model in version 2, which was based on the model given in *ICRP Publication 30* (*10*). Photon dose in both versions was based on the photon-specific absorbed fractions of Cristy and Eckerman for children and adults (*6*). The model used in version 3 was a significant departure from that used in version 2 both in terms of the numerical values estimated and capability.

The ICRP 30 model for electron dosimetry of bone and marrow was based somewhat on the work of Spiers et al. (*16*), but was generally very conservative and had little dependence on energy. Basically, a conservatively high value for the fraction of electron energy emitted in a source absorbed in a target was chosen to represent all energies. In the Eckerman model (*11*), the absorbed fractions were estimated at various energies. Then, the electron and/or beta spectrum for a radionuclide was folded over the absorbed fraction spectrum to produce dose conversion factors. In addition, the absorbed fraction spectrum was defined for several different bone groups in the body, permitting study of the absorbed dose to bone surfaces or marrow in different regions of the skeleton.

Knowledge of the fraction of marrow existing in different bones then permitted the expression of an absorbed dose distribution in histogram format. Therefore, in version 3 this new model was implemented and users were permitted use of the most recent photon- and electron-absorbed fractions. Users were also given the ability to look at marrow dose distributions and dose-volume histograms. An example of the output from the program showing this information is given in Figure 1. The residence times used to generate these results are those shown in Table 9.

Absorbed Dose to Small, Unit Density Spheres

Calculation of the absorbed dose to small, unit density spheres is often of interest, e.g., in the dose calculation to a tumor or to a small organ. Absorbed fractions for photons, given the assumption that the activity is distributed uniformly throughout the sphere, have been available for a number of years (*17,18*). Absorbed fractions for electrons and beta particles were recently published for a number of sphere sizes and emission energies (*19*). These datasets were combined in version 3 to permit the user to calculate S-values for any radionuclide in the program very easily (Fig. 2). An example of the output of this module is shown in Table 6.

RESULTS AND DISCUSSION

Tables 7–9 show a comparison of results generated by versions 2 and 3 for the reference adult phantom (70 kg), given a set of entered residence times. In Table 7, values for ^{14}C-glucose are shown. Carbon-14 is a pure beta emitter, and the model shown for ^{14}C-labeled glucose uses only four organs: the brain, liver, urinary bladder contents and remainder of the body.

The results between the two versions are virtually identical, with the exception of the dose to the bone marrow and bone surfaces. This is *not* due to the change in the bone and marrow model, but in the way that the dose from the remainder of the body to these organs is estimated.

In version 2, uniform activity in the remainder of the body was assumed to be uniform in marrow and bone and the absorbed fractions for electrons irradiating marrow and bone surfaces were applied to estimate S-values. In version 3, it was assumed that all organs should receive the same dose from activity uniform in the remainder of the body. This was the method employed in *MIRD Pamphlet No. 11*, and is a more reasonable approach.

Table 8 shows a comparison of results from the two codes for ^{99m}Tc-labeled MIBI (methoxyisobutyl isonitrile). The results are quite similar for all organs in this case.

Table 9 shows a comparison of results for a monoclonal antibody labeled with ^{131}I, which has some uptake in the red marrow and the bone. In this table, the differences between the

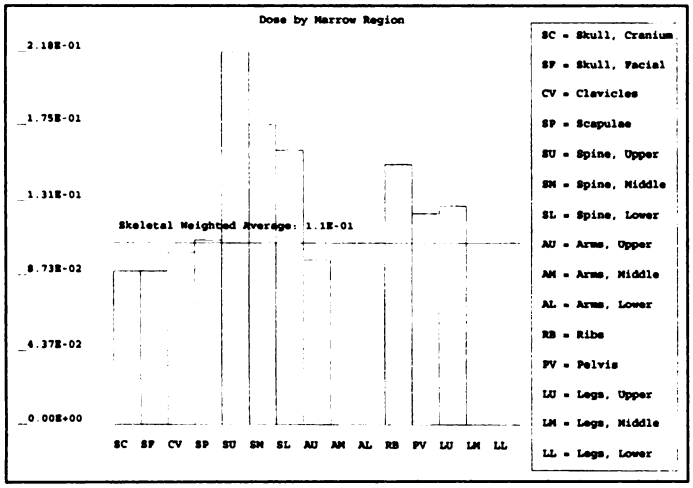

FIGURE 1. Sample of marrow dose report available in MIRDOSE versions 3.0 and 3.1. This plot shows marrow dose to different regions of the skeleton. On the computer screen, the histogram regions are shaded in different colors and on the printed output they are shown in different shades of grey (on a black and white printer) or color (on a color printer). For purposes of reproduction here, they are left unshaded.

uptake in the bone and marrow dose are clearly seen. All of the reasons for these differences will not be immediately clear from this example. The reader is directed to the paper by Eckerman and Stabin (*12*) for a more complete explanation of the new bone model and its differences from previous models.

Some minor differences may be noted for many other organs between the two codes. This may be attributed to a difference in the marrow mass between the two codes. MIRDOSE 2 uses a marrow mass of 1500 g, one which has been widely used and quoted.

MIRDOSE 3 uses a marrow mass of 1120 g, which was actually the original mass of active marrow suggested in *ICRP Publication 23* (*8*), whereas the value of 1500 g is the mass of marrow which contains some red marrow (but which actually also contains some yellow marrow). When this slight mass difference is introduced into the calculation for the remainder of the body S-value correction (Equation 2), the S-values for the remainder of the body to the different organs of the body become slightly higher, and thus the doses are increased slightly.

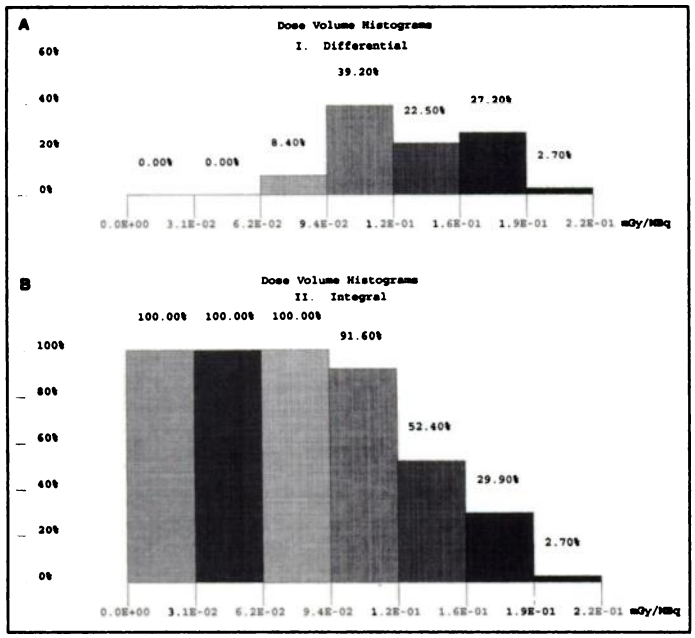

FIGURE 2. (A) Sample of the differential marrow dose volume histogram report available in MIRDOSE versions 3.0 and 3.1. This figure shows the fractions of marrow receiving absorbed doses between the values on the abscissa, based on the data in Figure 1 and assumed fractions of marrow in the different regions of the skeleton. On the computer screen, the histogram regions are shaded in different colors, and on the printed output, they are shown in different shades of grey (on a black and white printer) or color (on a color printer). (B) Sample of the integral marrow dose volume histogram report available in MIRDOSE version 3.0 and 3.1. This figure shows the fractions of marrow receiving absorbed doses greater than or equal to the values on the abscissa, based on the data in Figure 1 and assumed fractions of marrow in the different regions of the skeleton. On the computer screen, the histogram regions are shaded in different colors and on the printed output they are shown in different shades of grey (on a black and white printer) or color (on a color printer).

Effective Dose Equivalent and Effective Dose

In version 3, the quantities effective dose equivalent (*10*) and effective dose (*20*) were also calculated and added to the list of dose estimates given by the program. In theory, these quantities permit the representation of a nonuniform internal dose as a single value, which is the dose equivalent to that which the whole body could uniformly receive that would result in the same overall risk as the actual nonuniform dose distribution received. This may permit comparison of the radiation risk of different diagnostic agents (e.g., a ^{99m}Tc-labeled heart agent compared to ^{201}Tl) using a single number, or comparison of nuclear medicine and x-ray procedures, etc.

The two quantities—effective dose equivalent and effective dose—are identical in concept. They are different in name, in the numerical values of the organ risk weighting factors assigned (Table 10) and slightly different in the scheme used to estimate dose to remainder organs. Both values are given in version 3 for comparison and selection as the user chooses.

These quantities were originally designed for use in radiation protection programs (*10*), but their use has been suggested for nuclear medicine (*21–23*) by the ICRP (who designed it) and

TABLE 6
S-Values for Self-Irradiation: Small Unit Density Spheres, Iodine-131

Sphere mass (g)	Self-dose S-value (mGy/MBq-s)	Self-dose S-value (rad/μCi-hr)
0.01	2.34E+00*	3.11E+01*
0.10	2.70E−01*	3.60E+00*
0.50	5.70E−02*	7.59E−01*
1.00	2.95E−02	3.93E−01
2.00	1.50E−02	2.00E−01
4.00	7.64E−03	1.02E−01
6.00	5.16E−03	6.87E−02
8.00	3.89E−03	5.18E−02
10.00	3.13E−03	4.17E−02
20.00	1.58E−03	2.11E−02
40.00	8.10E−04	1.08E−02
60.00	5.55E−04	7.39E−03
80.00	4.26E−04	5.68E−03
100.00	3.45E−04	4.59E−03
300.00	1.21E−04	1.61E−03
400.00	9.23E−05	1.23E−03
500.00	7.49E−05	9.97E−04
600.00	6.30E−05	8.39E−04
1000.00	3.90E−05	5.20E−04
2000.00	2.05E−05	2.73E−04
3000.00	1.41E−05	1.88E−04
4000.00	1.09E−05	1.45E−04
5000.00	8.89E−06	1.18E−04
6000.00	7.55E−06	1.01E−04

*Electron/beta only.

TABLE 7
Comparison of MIRDOSE Versions 2 and 3 Results: Pure Beta Emitter in Four Organs: Carbon-14-Labeled Glucose

Target organ	Estimated radiation dose (mGy/MBq) MIRDOSE 2	MIRDOSE 3
Adrenals	2.47E−02	2.47E−02
Brain	3.17E−02	3.17E−02
Breasts	2.47E−02	2.47E−02
Gallbladder wall	2.47E−02	2.47E−02
LLI wall	2.47E−02	2.47E−02
Small intestine	2.47E−02	2.47E−02
Stomach	2.47E−02	2.47E−02
ULI wall	2.47E−02	2.47E−02
Heart wall	2.47E−02	2.47E−02
Kidneys	2.47E−02	2.47E−02
Liver	4.91E−02	4.91E−02
Lungs	2.47E−02	2.47E−02
Muscle	2.47E−02	2.47E−02
Ovaries	2.47E−02	2.47E−02
Pancreas	2.47E−02	2.47E−02
Red marrow	3.24E−02	2.47E−02
Bone surfaces	2.21E−02	2.47E−02
Skin	2.47E−02	2.47E−02
Spleen	2.47E−02	2.47E−02
Testes	2.47E−02	2.47E−02
Thymus	2.47E−02	2.47E−02
Thyroid	2.47E−02	2.47E−02
Urinary bladder wall	5.45E−02	5.46E−02
Uterus	2.47E−02	2.47E−02
Total body	2.55E−02	2.55E−02
Effective dose equivalent	2.93E−02*	2.84E−02
Residence times		
Brain	1.58E+00 hr	
Liver	3.29E+00 hr	
Urinary bladder contents	6.25E−01 hr	
Remainder of the body	6.08E+01 hr	

*Effective dose equivalent not available in version 2, but calculated based on the estimated organ doses.

TABLE 8
Comparison of MIRDOSE Versions 2 and 3 Results: Photon and Electron Emitter in Several Organs: Technetium-99m-MIBI*

Target organ	Estimated radiation dose (mGy/MBq) MIRDOSE 2	MIRDOSE 3
Adrenals	6.26E−03	6.25E−03
Brain	1.83E−03	1.83E−03
Breasts	1.85E−03	1.85E−03
Gallbladder wall	2.96E−02	2.96E−02
LLI wall	4.19E−01	4.20E−01
Small intestine	7.11E−02	7.09E−02
Stomach	1.28E−02	1.28E−02
ULI wall	1.70E−01	1.70E−01
Heart wall	4.96E−03	4.95E−03
Kidneys	2.31E−02	2.31E−02
Liver	8.21E−03	8.19E−03
Lungs	2.75E−03	2.75E−03
Muscle	8.82E−03	8.81E−03
Ovaries	6.25E−02	6.24E−02
Pancreas	8.78E−03	8.77E−03
Red marrow	1.25E−02	1.24E−02
Bone surfaces	1.30E−02	1.31E−02
Skin	3.40E−03	3.39E−03
Spleen	8.63E−03	8.62E−03
Testes	7.91E−03	7.90E−03
Thymus	2.46E−03	2.46E−03
Thyroid	2.22E−03	2.22E−03
Urinary bladder wall	5.37E−02	5.37E−02
Uterus	3.39E−02	3.39E−02
Total body	1.08E−02	1.07E−02
Effective dose equivalent	6.31E−02†	6.31E−02
Residence times		
Gallbladder contents	7.35E−02 hr	
Lower large intestine contents	8.86E+00 hr	
Small intestine contents	1.48E+00 hr	
Upper large intestine contents	4.80E+00 hr	
Heart wall	5.30E−02 hr	
Kidneys	2.90E−01 hr	
Liver	1.86E−01 hr	
Lungs	4.90E−02 hr	
Spleen	2.40E−02 hr	
Urinary bladder contents	7.80E−01 hr	
Remainder of the body	3.86E+00 hr	

*Methoxyisobutyl isonitrile.
†Effective dose equivalent not available in version 2, but calculated based on the estimated organ doses.

others. There is some controversy about the use of these quantities at the time of this writing (*24,25*), but the quantities are calculated in MIRDOSE 3 and offered to the user, in case they are of interest.

CONCLUSION

The MIRDOSE computer software greatly facilitates the calculation of internal radiation dose estimates by the MIRD technique. The user need only calculate organ residence times, enter them into the program and radiation dose estimates for all organs are estimated, including the effective dose equivalent and effective dose (in version 3). The program makes use of standard and most up-to-date models used in internal dosimetry. This results in standardization of dose estimates calculated from a given set of residence times, and should greatly enhance the ability of users, manufacturers, regulators and others to interpret radiation dose estimates.

Finally, it should be made clear that this program is in no way associated with the MIRD Committee of the Society of Nuclear Medicine. The name of the program implies only that it uses the MIRD technique. The MIRD Committee wishes it to be known that it does not endorse the MIRDOSE program, its input data, methods or results.

ACKNOWLEDGMENTS

This work was performed for the U.S. Department of Energy under contract DE-AC05-76OR00033 and for the U.S. Food and Drug Administration under Interagency Agreement No. FDA 224-75-3016, DOE 40-286-71. This article has been authored by a contractor of the U.S. Government under contract DE-AC05-76OR00033. Accordingly, the U.S. Government retains a nonexclusive, royalty-free license to publish or reproduce the published form of the contribution, or allow others to do so, for U.S. Government purposes.

TABLE 9
Comparison of MIRDOSE Versions 2 and 3 Results: Photon and Electron Emitter in Several Organs, Including the Red Marrow and Bone: Iodine-131-Labeled Monoclonal Antibody

Target organ	Estimated radiation dose (mGy/MBq) MIRDOSE 2	MIRDOSE 3
Adrenals	4.16E−02	4.19E−02
Brain	9.25E−03	9.47E−03
Breasts	8.77E−03	9.16E−03
Gallbladder wall	2.78E−02	2.83E−02
LLI wall	1.62E−02	1.67E−02
Small intestine	2.05E−02	2.10E−02
Stomach	1.95E−02	2.00E−02
ULI wall	1.98E−02	2.02E−02
Heart wall	1.38E−02	1.43E−02
Kidneys	1.57E+00	1.56E+00
Liver	4.68E−02	4.68E−02
Lungs	1.29E−02	1.32E−02
Muscle	1.38E−02	1.42E−02
Ovaries	1.69E−02	1.74E−02
Pancreas	3.15E−02	3.19E−02
Red marrow	1.92E−01	1.07E−01
Bone surfaces	2.65E−01	9.93E−02
Skin	9.40E−03	9.72E−03
Spleen	5.87E−02	5.88E−02
Testes	9.63E−03	1.01E−02
Thymus	1.02E−02	1.07E−02
Thyroid	9.58E−03	9.95E−03
Urinary bladder wall	1.34E−01	1.34E−01
Uterus	1.83E−02	1.88E−02
Total body	2.51E−02	2.51E−02
Effective dose equivalent	1.49E−01*	1.34E−01
Residence times		
Kidneys	3.71E+00 hr	
Liver	4.17E−01 hr	
Red marrow	1.50E+00 hr	
Cortical bone	5.00E−01 hr	
Trabecular bone	5.00E−01 hr	
Spleen	4.17E−02 hr	
Urinary bladder contents	4.00E−01 hr	
Remainder of the body	2.60E+00 hr	

*Effective dose equivalent not available in version 2, but calculated based on the estimated organ doses.

TABLE 10
Comparison of Organ Risk Weighting Factors for Effective Dose Equivalent and Effective Dose

Organ	Effective dose equivalent (ICRP 30)	Effective dose (ICRP 60)
Gonads	0.25	0.20
Red marrow	0.12	0.12
Colon	—	0.12
Lungs	0.12	0.12
Stomach	—	0.12
Bladder	—	0.05
Breasts	0.15	0.05
Liver	—	0.05
Esophagus	—	0.05
Thyroid	0.03	0.05
Skin	—	0.01
Bone surfaces	0.03	0.01
Remainder	0.30*	0.05†

*The weighting factor for the remainder in the effective dose equivalent is to be divided equally among the five highest organs not explicitly mentioned in this list which receive the highest absorbed doses.

†The weighting factor for the remainder in the effective dose is to be divided equally among ten organs not explicitly mentioned in this list but which were assigned by the ICRP (adrenals, brain, ULI, small intestine, kidneys, muscle, pancreas, spleen, thymus and uterus).

REFERENCES

1. Loevinger R, Budinger T, Watson E. *MIRD primer for absorbed dose calculations.* New York: Society of Nuclear Medicine; 1988.
2. Watson E, Stabin M. Basic alternative software package for internal radiation dose calculations. In: Kathren RL, Higby DP, McKinney MA, eds. *Computer applications in health physics. Proceedings of the 17th Midyear Topical Symposium of the Health Physics Society.* Richland, WA; 1984.
3. Weber D, Eckerman KF, Dillman LT, Ryman J. *MIRD: radionuclide data and decay schemes.* New York: Society of Nuclear Medicine; 1989.
4. Kocher D. *Radioactive Decay Data Tables*, Oak Ridge National Laboratories, Oak Ridge, Tennessee. 1981. DOE/TIC-11026.
5. ICRP Publication 38. *Radionuclide transformations—energy and intensity of emissions.* Oxford: Pergamon Press; 1983.
6. Cristy M, Eckerman K. Specific absorbed fractions of energy at various ages from internal photons sources. *ORNL/TM-8381 V1–V7.* Oak Ridge, TN: Oak Ridge National Laboratory; 1987.
7. Stabin M, Watson E, Cristy M, et al. Mathematical models of the adult female at various stages of pregnancy. *ORNL Report ORNL/TM-12907.* Oak Ridge, TN: Oak Ridge National Laboratory; 1995: in press.
8. International Commission on Radiological Protection. *Report of the Task Group on Reference Man*, ICRP Publication 23. New York: Pergamon Press; 1975.
9. Snyder W, Ford M, Warner G, Watson S. *"S," absorbed dose per unit cumulated activity for selected radionuclides and organs*, MIRD Pamphlet No. 11. New York: Society of Nuclear Medicine; 1975.
10. International Commission on Radiological Protection. *Limits for intakes of radionuclides by workers*, ICRP Publication 30. New York: Pergamon Press; 1979.
11. Eckerman KF. Aspects of dosimetry of radionuclides within the skeleton with particular emphasis on the active marrow. In: *Fourth International Radiopharmaceutical Dosimetry Symposium*; Schlafke-Stelson AT and Watson EE, eds. CONF-851113, Oak Ridge, TN: Oak Ridge Associated Universities; 1986:514–534.
12. Eckerman K, Stabin M. Dose conversion factors for marrow and bone by skeletal regions [Abstract]. *J Nucl Med* 1995;36:1994;35:112P.
13. Cloutier R, Watson E, Rohrer R, Smith E. Calculating the radiation dose to an organ, *J Nucl Med* 1973;14:53–55.
14. Draper N, Smith H. *Applied regression analysis.* New York: John Wiley & Sons; 1966:7–13.
15. Cloutier R, Smith S, Watson E, Snyder W, Warner G. Dose to the fetus from radionuclides in the bladder. *Health Phys* 1973;25:147–161.
16. Spiers FW. Beta dosimetry in trabecular bone. In: Mays CW, ed. *Delayed effects of bone-seeking radionuclides* Salt Lake City, UT: University of Utah Press; 1969:95–108.
17. Brownell G, Ellett W, Reddy R. MIRD pamphlet no. 3—absorbed fractions for photon dosimetry. *J Nucl Med* 1968;27(suppl):37.
18. Ellett W, Humes R. MIRD pamphlet no. 8—absorbed fractions for small volumes containing photon-emitting radioactivity. *J Nucl Med* 1972;13(suppl):30.
19. Siegel JA, Stabin MG. Absorbed fractions for electrons and beta particles in small spheres [Abstract]. *J Nucl Med* 1988;29:803.
20. International Commission on Radiological Protection. *1990 recommendations of the International Commission on Radiological Protection*, ICRP Publication 60. New York: Pergamon Press; 1991.
21. International Commission on Radiological Protection. *Protection of the patient in nuclear medicine*, ICRP Publication 52. New York: Pergamon Press; 1987.
22. International Commission on Radiological Protection. *Radiation dose to patients from radiopharmaceuticals*, ICRP Publication 53. New York: Pergamon Press; 1988.
23. United Nations Scientific Committee on the Effects of Atomic Radiation. *Sources and effects of ionizing radiation*, UNSCEAR 1993 Report to the General Assembly. New York: United Nations; 1993.
24. Poston J. Application of the effective dose equivalent to nuclear medicine patients. *J Nucl Med* 1993;34:714–716.
25. Stabin M, Stubbs J, Watson E. Recent controversy in radiation dosimetry. *Eur J Nucl Med* 1993;20:371–372.